Avrupa Bilim ve Teknoloji Dergisi
Sayı 35, S. 168-176, Nisan 2022

Araştırma Makalesi

www.ejosat.com ISSN:2148-2683

European Journal of Science and Technology
No. 35, pp. 168-176, April 2022

Research Article

A Novel Selective Mapping Method based on Cumulative Symbol Optimization for PAPR Minimization in Low Complexity GFDM Transmitter

Şakir Şimşir[1*], Necmi Taşpınar[2]

[1*] Nevşehir Hacı Bektaş Veli University, Faculty of Engineering and Architecture, Departmant of Electrical and Electronics Engineering, Nevşehir, Turkey, (ORCID: 0000-0002-1287-160X), sakirsimsir@nevsehir.edu.tr

[2] Erciyes University, Faculty of Engineering, Departmant of Electrical and Electronics Engineering, Kayseri, Turkey, (ORCID: 0000-0003-4689-4487), taspinar@erciyes.edu.tr

(First received 23 February 2022 and in final form 25 March 2022)

(**DOI:** 10.31590/ejosat.1078288)

ATIF/REFERENCE: Şimşir, Ş. & Taşpınar, N. (2022). A Novel Selective Mapping Method based on Cumulative Symbol Optimization for PAPR Minimization in Low Complexity GFDM Transmitter. *European Journal of Science and Technology*, (35), 168-176.

Abstract

In this paper, the problem of high peak-to-average power ratio (PAPR) in the low complex version of the generalized frequency division multiplexing (LC-GFDM) is handled by developing a novel PAPR reduction method called cumulative symbol optimization-selective mapping (CSO-SLM). With this new method, the disadvantage caused by the symbol addition process that greatly reduces the SLM performance in the LC-GFDM transmitter was eliminated thanks to the combination of SLM technique with the cumulative symbol optimization procedure. In order to demonstrate the benefit of integrating the CSO procedure into the SLM scheme, our proposed CSO-SLM strategy was compared to the conventional SLM technique with regard to both PAPR reduction and power spectral density (PSD) performance in the simulations. Moreover, the CSO-partial transmit sequence (CSO-PTS) technique, which was specially developed for the LC-GFDM system as the CSO-SLM strategy, and a robust PAPR reduction method named GreenOFDM were also used for comparison. According to the simulation results, the proposed CSO-SLM technique clearly outperforms each of the benchmark strategies considered in this paper by leaving them behind with regard to the amounts of PAPR and PSD improvements achieved in the LC-GFDM transmission signal.

Keywords: PAPR, LC-GFDM, 5G, Cumulative symbol optimization, Selective mapping.

Düşük Karmaşıklı GFDM Vericisinde PAPR Minimizasyonu için Birikimli Sembol Optimizasyonuna Dayalı Yeni Bir Seçici Eşleme Yöntemi

Öz

Bu çalışmada, birikimli sembol optimizasyonu-seçici eşleme (CSO-SLM) adı verilen yeni bir PAPR düşürme yöntemi geliştirilerek, genelleştirilmiş frekans bölmeli çoğullamanın düşük karmaşıklı versiyonundaki (LC-GFDM) yüksek tepe gücü/ortalama güç oranı problemi ele alınmıştır. Bu yeni yöntemle birlikte, SLM tekniğinin birikimli sembol optimizasyon prosedürü ile birleştirilmesi sayesinde, LC-GFDM vericisinde SLM performansını büyük ölçüde düşüren sembollerin toplanması işleminin yol açtığı dezavantaj ortadan kaldırılmıştır. CSO prosedürünü SLM şemasına entegre etmenin faydasını göstermek amacıyla, önermiş olduğumuz CSO-SLM stratejisi geleneksel SLM tekniği ile simülasyonlarda hem PAPR düşürme hem de güç spektral yoğunluğu (PSD) performansı bakımından karşılaştırılmıştır. Ayrıca, LC-GFDM sistemi için CSO-SLM stratejisi gibi özel olarak geliştirilmiş olan CSO-kısmi iletim dizisi (CSO-PTS) tekniği ve GreenOFDM isimli güçlü bir PAPR düşürme yöntemi de karşılaştırma amaçlı kullanılmıştır. Simülasyon sonuçlarına göre, önerilen CSO-SLM yöntemi, bu çalışmada ele alınan kıyaslama stratejilerini LC-GFDM iletim sinyalinde elde edilen PAPR ve PSD iyileştirme miktarları bakımından geride bırakarak her birinden net olarak daha iyi bir performans göstermiştir.

Anahtar Kelimeler: PAPR, LC-GFDM, 5G, Birikimli sembol optimizasyonu, Seçici eşleme.

[*] Corresponding Author: sakirsimsir@nevsehir.edu.tr

1. Introduction

Due to its unique features, it didn't take long for generalized frequency division multiplexing (GFDM) (Fettweis et al., 2009) to find its way into the fifth generation (5G) and beyond candidate waveforms considered to have the potential of replacing the orthogonal frequency division multiplexing (OFDM) (Cimini, 1985; Taşpınar and Şimşir, 2020; Güner, 2022) being utilized in the current fourth generation (4G) Long-Term Evolution systems. In the GFDM system, each subcarrier is filtered by means of a prototype filter circularly shifted in both frequency and time domain. This filtering operation makes it possible to reduce the out of band emission and carry out dynamic spectrum allocation without allowing serious interference among the users. Apart from this, the transmission signals with high frequency localization characteristics can be obtained in the GFDM system owing to the employment of adjustable filters at the transmitter side. Moreover, both frequency and time domain multiuser scheduling are possible in the GFDM (Fettweis et al., 2009; Michailow et al., 2012; Michailow et al., 2014; Michailow et al., 2012).

On the other hand, not long after the presentation of the GFDM waveform to the science community, its low complex version called low complexity-GFDM (LC-GFDM) (Matthé et al., 2016) was developed. In this new GFDM variant, the generation of transmission signal and the acquisition of the information data from the received signal can be performed with lower processing load in comparison to the original GFDM system. However, the usage of multicarrier transmission strategy in the LC-GFDM scheme brings about the generation of transmission signals with high peak-to-average power ratio (PAPR) just as in the OFDM, GFDM and the other multicarrier waveforms. It is an undesired situation in wireless communication that the transmission signals reach high PAPR levels. Because these signals have to be amplified via a type of nonlinear high power amplifier (HPA) (Paredes et al., 2017; Ryu et al., 2004) before transmission and if the transmission signal given to the input of nonlinear HPA has high PAPR value, it cannot be amplified without serious distortions, which result in out of band radiation as well. With a view to get rid of high PAPR problem and its negative consequences in wireless communication, wide variety of PAPR reduction strategies were developed in the literature. The most famous and frequently used ones can be collocated as follows; coding (Jones et al., 1994), clipping and filtering (Li and Cimini, 1998), tone injection (TI) (Chen and Wen, 2010), selective mapping (SLM) (Bauml et al., 1996), active constellation extension (ACE) (Krongold and Jones, 2003), partial transmit sequence (PTS) (Cimini and Sollenberger, 2000), tone reservation (TR) (Krongold and Jones, 2004) and interleaving (Jayalath and Tellambura, 2000).

Each of the aforementioned PAPR reduction strategies has specific benefits. Nevertheless, some distinguishing features makes some methods to be preferred more frequently. SLM technique is one of them. One of the most significant superiorities of the SLM scheme is to have the capacity of PAPR alleviation without allowing any information lost in the transmission signals. The other notable feature that boosts the preference frequency of SLM in PAPR reduction studies is possessing the structure that is suitable for both hybridization and modification operations. On the other hand, in case of applying the SLM scheme, which was actually proposed for the OFDM system, directly to the transmitter of LC-GFDM, the related scheme suffers a huge loss of performance because of the signal generation mechanism existing in the LC-GFDM transmitter where the GFDM data vectors are multiplied by the impulse responses of the transmitter filter, which are shifted circularly in time domain, to obtain the GFDM symbols. These symbols are then aggregated to attain the eventual transmission signal of the LC-GFDM system. Since the SLM technique follows a procedure in which the symbols are considered independently of each other and the PAPR value of every single symbol is reduced without taking the other symbols into consideration, direct application of SLM scheme to the transmitter of LC-GFDM will provide individual PAPR alleviation among the GFDM symbols but PAPR re-growth will be seen in the eventual transmission signal because of the symbol summing operation carried out at the end of LC-GFDM transmitter. In consideration of the related symbol addition procedure, a new SLM scheme based on cumulative symbol optimization (CSO-SLM) was developed for PAPR minimization in the LC-GFDM system. In this new scheme, the PAPR of GFDM symbols are reduced in order. However, when reducing the PAPR of any symbol, the summation of previously optimized GFDM symbols is taken into account. As the optimization process progresses from the first to the last GFDM symbol, the number of symbols taken into consideration for the optimization of current symbol augments in a cumulative way. In this manner, the performance deterioration caused by the symbol addition process on the conventional SLM technique is eliminated.

When looking at the literature, it will be seen that there is only one PAPR reduction study (Şimşir and Taşpınar, 2020) carried out for the LC-GFDM system. In (Şimşir and Taşpınar, 2020), cumulative symbol optimization procedure was developed for the first time and integrated to the conventional PTS scheme to create CSO-PTS strategy for PAPR lowering in the LC-GFDM system. On the other hand, it is possible to come across some studies in the literature concerning the PAPR lowering in the original GFDM waveform as follows (Tiwari and Paulus, 2020; Jayati et al., 2019; Sim et al., 2019; Barba-Maza and Dolecek, 2020): In (Tiwari and Paulus, 2020), the PAPR of transmission signal generated by the GFDM system was reduced using the nonlinear companding technique together with the clipping method. In (Jayati et al., 2019), both PTS and SLM techniques were applied to the GFDM waveform, and PAPR reduction performances of these techniques were compared. In (Sim et al., 2019), a pulse shaping filter designed by employing an effective optimization technique was suggested to reduce PAPR in the GFDM scheme. In (Barba-Maza and Dolecek, 2020), in order to carry out PAPR reduction process without increasing the symbol error rate in the GFDM system, it was proposed to use the overlapping PTS method together with the fourth-order Xia pulse.

The main contributions of this study are as follows:

1. The cumulative symbol optimization procedure was applied to the SLM scheme for the first time to develop a novel PAPR reduction strategy called CSO-SLM for the LC-GFDM system.
2. Thanks to the integration of cumulative symbol optimization mechanism to the classical SLM scheme, the PAPR reduction performance of the related scheme in the LC-GFDM system was upgraded, significantly.
3. Our proposed CSO-SLM strategy clearly outperforms both CSO-PTS (Şimşir and Taşpınar, 2020) and

GreenOFDM (Mestdagh et al., 2018) techniques considered in this paper.

The remaining part of the paper is organized as follows: In Section 2, LC-GFDM system is described and PAPR of transmission signal in the related system is defined. In Section 3, conventional SLM method is presented. In Section 4, our proposed CSO-SLM strategy is explained step by step. Finally, in Section 5 and Section 6, the simulation results and conclusions are given, respectively.

2. Description of LC-GFDM System

Figure 1 illustrates the operations required for generating the LC-GFDM transmission signal (Matthé et al., 2016; Şimşir and Taşpınar, 2020). As obviously seen from the Figure 1, the first action to be carried out in the process of signal generation is mapping the information bits (*b*) to quadrate amplitude modulation (QAM) symbols. After the QAM mapping operation, the resulting *N*-length data sequence (*d*) is split into *K*-length data vectors defined as follows (Matthé et al., 2016; Şimşir and Taşpınar, 2020):

$$d_m = \left[d_{0,m}\, ,\, d_{1,m}\, ,\ldots, d_{K-1,m} \right] \quad , \quad 1 \le m \le M \tag{1}$$

where *M* denotes the number of *K*-length data sequences. Later on, inverse fast Fourier transform (IFFT) is applied to each of the related data sequences in the following way (Matthé et al., 2016; Şimşir and Taşpınar, 2020):

$$d_m[n] = \frac{1}{\sqrt{K}} \sum_{k=0}^{K-1} d_{k,m} e^{\frac{j2\pi kn}{K}} \quad , \quad 0 \le n \le K-1 \tag{2}$$

Following the IFFT operation, each sequence of $d_m[n]$ is replicated *M* times. After that, the resulting replicas are lined up to obtain $c_m[n]$ sequences, each of which has the length of $N = MK$, as follows (Matthé et al., 2016; Şimşir and Taşpınar, 2020):

$$c_m[n] = \left[\overbrace{\left[d_m[0], d_m[1], \ldots, d_m[K-1] \right]}^{1}, \overbrace{\left[d_m[0], d_m[1], \ldots, d_m[K-1] \right]}^{2} , \ldots , \overbrace{\left[d_m[0], d_m[1], \ldots, d_m[K-1] \right]}^{M} \right] \quad , \quad 0 \le n \le MK-1 \tag{3}$$

Eventually, the signal to be transmitted is acquired in the following manner (Matthé et al., 2016; Şimşir and Taşpınar, 2020):

$$s[n] = \sum_{m=1}^{M} g\left[\left\langle n-(m-1)K \right\rangle_N \right] c_m[n] \quad , \quad 0 \le n \le MK-1 \tag{4}$$

In the expression above, impulse response of the prototype filter denoted by $g[n]$ is circularly shifted for each *m* value by using the modulo operator $\langle \bullet \rangle_N$.

2.1. Definition of PAPR for the LC-GFDM Transmission Signal

The accurate PAPR results for the LC-GFDM transmission signals in discrete-time cannot be achieved without the oversampling operation. For this reason, as a first step, the oversampled versions of the $d_m[n]$ data sequences have to be obtained in the following way (Şimşir and Taşpınar, 2020):

$$d_m[n] = \frac{1}{\sqrt{K}} \sum_{k=0}^{K-1} d_{k,m} e^{\frac{j2\pi kn}{LK}} \quad , \quad 0 \le n \le LK-1 \tag{5}$$

After *M*-times copying of the resulting $d_m[n]$ sequences oversampled by the factor *L*, the time domain concatenation process of the relevant copies is performed as follows (Şimşir and Taşpınar, 2020):

$$c_m[n] = \left[\overbrace{\left[d_m[0], d_m[1], \ldots, d_m[LK-1] \right]}^{1}, \overbrace{\left[d_m[0], d_m[1], \ldots, d_m[LK-1] \right]}^{2} , \ldots , \overbrace{\left[d_m[0], d_m[1], \ldots, d_m[LK-1] \right]}^{M} \right] \quad , \quad 0 \le n \le MLK-1 \tag{6}$$

Subsequent to the acquisition of $c_m[n]$ sequences via the concatenation process, the last operation defined below is put into practice to achieve the final transmission signal (Şimşir and Taşpınar, 2020):

$$s[n] = \sum_{m=1}^{M} g\left[\left\langle n-(m-1)LK \right\rangle_{LN} \right] c_m[n] \quad , \quad 0 \le n \le MLK-1 \tag{7}$$

The operations carried out in the Equation (7) to generate the transmission signal $s[n]$ is expressed visually in Figure 2 (Şimşir and Taşpınar, 2020). Herewith, the definition of PAPR for the $s[n]$ signal is made in the following manner (Şimşir and Taşpınar, 2020):

$$PAPR\left(s[n]\right) = 10\log_{10} \frac{\max\limits_{0 \le n \le MLK-1} \left[\left| s[n] \right|^2 \right]}{E\left[\left| s[n] \right|^2 \right]} \left(dB \right) \tag{8}$$

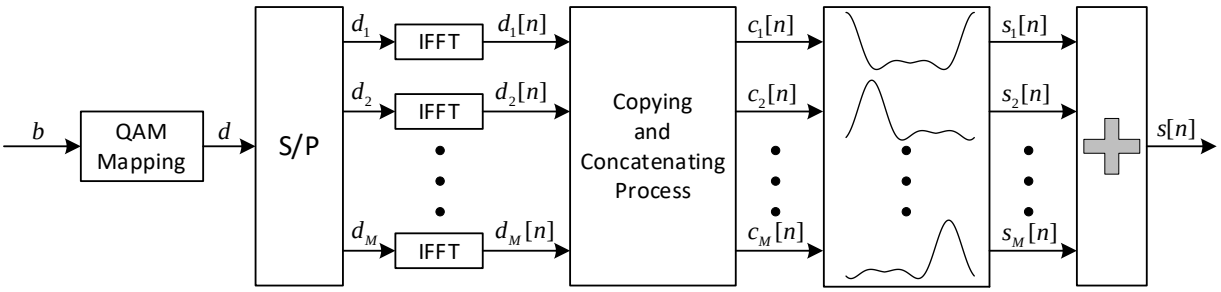

Figure 1. LC-GFDM block diagram.

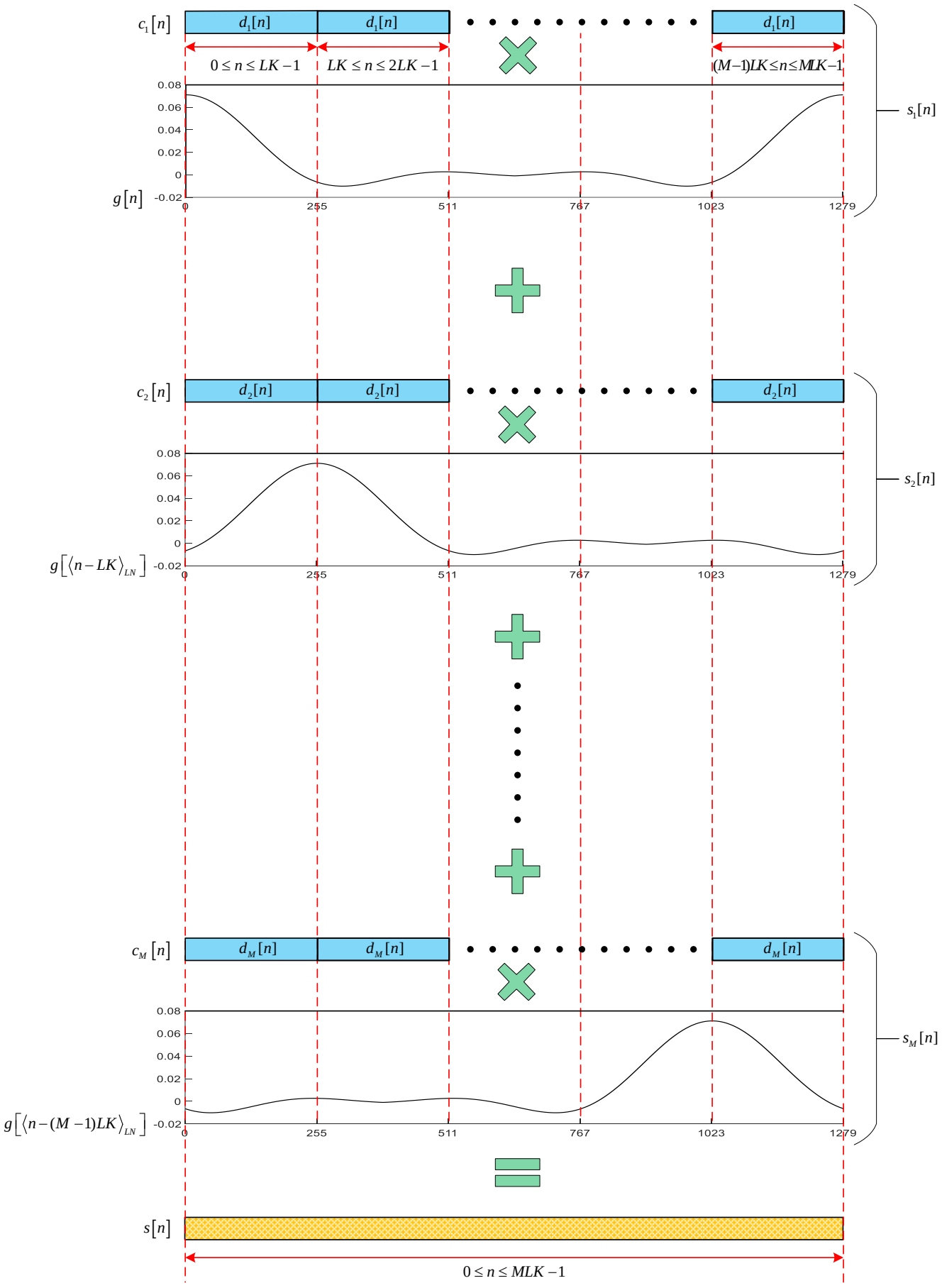

Figure 2. The illustration of generating LC-GFDM signal (L = 8, K = 32, M = 5, prototype filter: root raised cosine (rrc), roll-off factor (α) = 0.5).

3. Conventional SLM Method

The demonstration of SLM-based PAPR minimization process is given in Figure 3 (Bauml et al., 1996). As it is quite clear in the Figure 3, first of all, *U* different phase sequences, each of which has the length *K*, is generated in a random way to carry out phase rotation process in the input vector defined as $X=[X_0, X_1, ..., X_{K-1}]$. These randomly generated phase sequences are expressed in the following manner (Bauml et al., 1996):

$$b^{(u)}=\left[b_0^{(u)},\ b_1^{(u)},...,b_{K-1}^{(u)}\right] \quad , \qquad u=0,1,...,U-1 \tag{9}$$

where $b_k^{(u)} \in \{-1,+1\}$, $k=0,1,...,K-1$. Subsequently, phase rotation process is put into practice by performing an element-wise multiplication between the vector *X* and the randomly generated phase sequences as follows (Bauml et al., 1996):

$$\begin{aligned} X^{(u)} &= \left[X_0 \cdot b_0^{(u)},\ X_1 \cdot b_1^{(u)},...,X_{K-1} \cdot b_{K-1}^{(u)}\right] \\ &= \left[X_0^{(u)},\ X_1^{(u)},...,X_{K-1}^{(u)}\right] \end{aligned} \tag{10}$$

where $X^{(u)}$ represents the *u*th data sequence acquired via the multiplication of vector *X* by the *u*th phase sequence symbolized by $b_k^{(u)}$. After that, the oversampled time domain versions of the $X^{(u)}$ vectors are obtained as follows (Bauml et al., 1996):

$$x^{(u)}[n]=IFFT\left(X^{(u)}\right)=\frac{1}{\sqrt{K}}\sum_{k=0}^{K-1}X_k \cdot b_k^{(u)} \cdot e^{\frac{j2\pi kn}{LK}}, \tag{11}$$

$$0 \le n \le LK-1$$

Finally, among the candidate $x^{(u)}[n]$ signals, the one possessing smallest PAPR value is chosen for transmission. The sequence of phase factors utilized in the generation of the selected candidate signal is determined as the optimum phase sequence. The main goal of SLM strategy is to reach the optimum phase sequence that produces the signal $x'[n]$ with the lowest PAPR in *U* different trials in each of which a random phase sequence is generated.

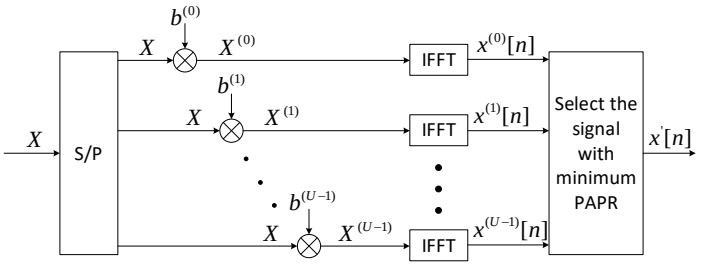

Figure 3. Block diagram of the conventional SLM scheme.

4. The CSO-SLM Strategy

When reducing the PAPR by using the classical SLM technique, each symbol is handled independently from the other ones without taking into account the interaction between them. However, the summation of the PAPR-reduced symbols for the generation of LC-GFDM transmission signal leads to a significant re-growth in the PAPR of total signal. To put it more clearly, the signal generation mechanism of the LC-GFDM system adversely affects the performance of classical SLM scheme. For this reason, the cumulative symbol optimization procedure developed for eliminating the PAPR-increasing consequence of the symbol addition operation in (Şimşir and Taşpınar, 2020) was integrated to the classical SLM scheme. By doing so, the new PAPR reduction strategy called CSO-SLM was developed. Together with the aforementioned modification, the conventional SLM technique has become more compatible with the LC-GFDM system and its PAPR reduction capability in the related system has increased. The steps of the CSO-SLM strategy are given below:

Step 1: At the beginning, the first GFDM symbol $s_1[n]$ is optimized. Towards that end, as an initial operation, *U* different phase sequences are generated, randomly for the first data vector $d_1=\left[d_{0,1},\ d_{1,1},...,d_{K-1,1}\right]$. The phase sequences generated for the first data vector is defined as follows:

$$b_1^{(u)}=\left[b_{0,1}^{(u)},\ b_{1,1}^{(u)},...,b_{K-1,1}^{(u)}\right] \quad , \qquad u=0,1,...,U-1 \tag{12}$$

It should be noted that $b_m^{(u)} \in \{-1,+1\}$. The vector d_1 is then multiplied by the phase sequences generated for it as follows:

$$\begin{aligned} d_1^{(u)} &= \left[d_{0,1} \cdot b_{0,1}^{(u)},\ d_{1,1} \cdot b_{1,1}^{(u)},...,d_{K-1,1} \cdot b_{K-1,1}^{(u)}\right] \\ &= \left[d_{0,1}^{(u)},\ d_{1,1}^{(u)},...,d_{K-1,1}^{(u)}\right] \end{aligned} \tag{13}$$

where $d_1^{(u)}$ is the phase rotated data sequence obtained by multiplying the vector d_1 by the *u*th phase sequence. The oversampled time domain version of the resulting $d_1^{(u)}$ sequence is acquired in the following way:

$$d_1^{(u)}[n]=\frac{1}{\sqrt{K}}\sum_{k=0}^{K-1}d_{k,1}^{(u)}e^{\frac{j2\pi kn}{LK}} \quad , \quad 0 \le n \le LK-1 \tag{14}$$

Step 2: The sequence of $d_1^{(u)}[n]$ is replicated *M* times. The relevant replicas of $d_1^{(u)}[n]$ are then arranged side by side as follows:

$$\begin{aligned} c_1^{(u)}[n] = \Bigg[& \overbrace{\left[d_1^{(u)}[0], d_1^{(u)}[1], ..., d_1^{(u)}[LK-1]\right]}^{1}, \overbrace{\left[d_1^{(u)}[0], d_1^{(u)}[1], ..., d_1^{(u)}[LK-1]\right]}^{2} \\ & , ..., \overbrace{\left[d_1^{(u)}[0], d_1^{(u)}[1], ..., d_1^{(u)}[LK-1]\right]}^{M} \Bigg] \quad , \quad 0 \le n \le MLK-1 \end{aligned} \tag{15}$$

Step 3: $c_1^{(u)}[n]$ vector obtained after fulfilling the side-by-side placement of $d_1^{(u)}[n]$ copies is filtered to achieve the first GFDM symbol as follows:

$$s_1^{(u)}[n]=g[n]c_1^{(u)}[n] \quad , \quad 0 \le n \le MLK-1 \tag{16}$$

Step 4: After that, optimal phase vector to be used in the phase rotation process of the first symbol is found through the following operation:

$$b_1^* = \arg \min_{b_1^{(u)}} \left\{ \max_{0 \le n \le MLK-1} \left| s_1^{(u)}[n] \right|^2 \right\} \tag{17}$$

Step 5: The optimal phase sequence b_1^* attained for the first symbol is utilized in the acquisition of the first optimized GFDM symbol denoted by $s_1^*[n]$ as follows:

$$d_1^* = \left[d_{0,1} \cdot b_{0,1}^*,\ d_{1,1} \cdot b_{1,1}^*, ..., d_{K-1,1} \cdot b_{K-1,1}^* \right] = \left[d_{0,1}^*,\ d_{1,1}^*, ..., d_{K-1,1}^* \right] \quad (18)$$

$$d_1^*[n] = \frac{1}{\sqrt{K}} \sum_{k=0}^{K-1} d_{k,1}^* e^{\frac{j2\pi kn}{LK}} \quad (19)$$

$$c_1^*[n] = \left[\overbrace{\left[d_1^*[0], d_1^*[1], ..., d_1^*[LK-1] \right]}^{1}, \overbrace{\left[d_1^*[0], d_1^*[1], ..., d_1^*[LK-1] \right]}^{2}, ..., \overbrace{\left[d_1^*[0], d_1^*[1], ..., d_1^*[LK-1] \right]}^{M} \right] \quad (20)$$

$$s_1^*[n] = g[n] c_1^*[n] \quad (21)$$

Step 6: $c_2^{(u)}[n]$ is obtained by repeating the Step 1 and Step 2 operations for the 2nd data vector defined as $d_2 = \left[d_{0,2}, d_{1,2}, ..., d_{K-1,2} \right]$. Afterwards, the 2nd GFDM symbol $s_2^{(u)}[n]$ is attained by applying the following operation to the vector $c_2^{(u)}[n]$.

$$s_2^{(u)}[n] = g\left[\langle n - LK \rangle_{LN} \right] c_2^{(u)}[n] \quad (22)$$

Step 7: For $s_2^{(u)}[n]$, the optimal phase sequence is found by taking into account the first optimized symbol $s_1^*[n]$ as follows:

$$b_2^* = \arg \min_{b_2^{(u)}} \left\{ \max_{0 \le n \le MLK-1} \left| s_1^*[n] + s_2^{(u)}[n] \right|^2 \right\} \quad (23)$$

Step 8: $s_2^*[n]$ denoting the second optimized GFDM symbol is achieved by using b_2^* in the following way:

$$d_2^* = \left[d_{0,2} \cdot b_{0,2}^*,\ d_{1,2} \cdot b_{1,2}^*, ..., d_{K-1,2} \cdot b_{K-1,2}^* \right] = \left[d_{0,2}^*,\ d_{1,2}^*, ..., d_{K-1,2}^* \right] \quad (24)$$

$$d_2^*[n] = \frac{1}{\sqrt{K}} \sum_{k=0}^{K-1} d_{k,2}^* e^{\frac{j2\pi kn}{LK}} \quad (25)$$

$$c_2^*[n] = \left[\overbrace{\left[d_2^*[0], d_2^*[1], ..., d_2^*[LK-1] \right]}^{1}, \overbrace{\left[d_2^*[0], d_2^*[1], ..., d_2^*[LK-1] \right]}^{2}, ..., \overbrace{\left[d_2^*[0], d_2^*[1], ..., d_2^*[LK-1] \right]}^{M} \right] \quad (26)$$

$$s_2^*[n] = g\left[\langle n - LK \rangle_{LN} \right] c_2^*[n] \quad (27)$$

Step 9: In this manner, the optimization of GFDM symbols is performed in turn until the *M*th symbol. When it comes to the symbol *M*, the optimal phase sequence for the related symbol is found by taking into account the sum of all the remaining GFDM symbols optimized up to the (M – 1)th symbol in the following way:

$$b_M^* = \arg \min_{b_M^{(u)}} \left\{ \max_{0 \le n \le MLK-1} \left| \sum_{m=1}^{M-1} s_m^*[n] + s_M^{(u)}[n] \right|^2 \right\} \quad (28)$$

where $s_M^{(u)}[n]$ corresponding to the *M*th GFDM symbol is expressed below:

$$s_M^{(u)}[n] = g\left[\langle n - (M-1)LK \rangle_{LN} \right] c_M^{(u)}[n] \quad (29)$$

Step 10: For the purpose of achieving the final LC-GFDM transmission signal with minimized PAPR, the following operation is put into practice in the last step:

$$s^*[n] = \sum_{m=1}^{M} g\left[\langle n - (m-1)LK \rangle_{LN} \right] c_m^*[n] = \sum_{m=1}^{M} s_m^*[n] \quad (30)$$

5. Simulation Results

In this section, the performance analysis of the CSO-SLM technique developed for the LC-GFDM system was carried out. In the related performance analysis, the CSO-SLM strategy was compared to both the classical SLM and GreenOFDM (Mestdagh et al., 2018), which is an SLM-based state of art PAPR reduction strategy proposed in recent years. In the last stage of the performance analysis, this time, the CSO-SLM strategy was compared to the CSO-PTS technique developed in (Şimşir and Taşpınar, 2020) specifically for the LC-GFDM system as our proposed method. The aforementioned comparisons were carried out on the basis of two main performance criteria. These are the PAPR reduction and power spectral density (PSD) performances, respectively.

In the PTS-based PAPR reduction techniques like PTS and CSO-PTS, a different combination of phase sequence is generated for each of the *SN* different searches carried out to find the optimum phase sequence for any symbol in the LC-GFDM system. Therefore, the value of parameter *SN* corresponding to the search number in these types of PAPR reduction strategies is also equal to the number of phase sequence combinations generated, randomly. In the SLM scheme and its modified versions such as CSO-SLM and GreenOFDM, a random combinations of phase factors are generated for each search as in the PTS-based PAPR reduction techniques. However, in such schemes, *U* different phase sequences defined as $b_m^{(u)} = \left[b_{m,0}^{(u)},\ b_{m,1}^{(u)}, ..., b_{m,K-1}^{(u)} \right]$, $u = 0,1,...,U-1$ are generated in total for *SN* number of searches. To put it more clearly, the equivalent of the *SN* parameter in the SLM-based PAPR lowering schemes is the parameter *U*. So, in order to avoid any confusion in the performance comparisons to be carried out for different number of searches between the PTS and SLM-based PAPR reduction strategies, the number of searches will be expressed by a single parameter. To this end, the parameter *SN* will be used to represent the number of searches for both SLM and PTS-based techniques in this section. Table 1 contains the parameter values belonging to the simulation studies.

Table 1. Simulation parameters.

Modulation type	4-QAM
Oversampling factor (*L*)	8
Size of FFT	256
Number of symbols (*M*)	9
Number of subcarriers (*K*)	32
HPA model	Solid state power amplifier (SSPA)
Type of transmitter filter	Root raised cosine (rrc)
Roll-off factor (α)	0.9
Number of sub-blocks in CSO-PTS (*V*)	8

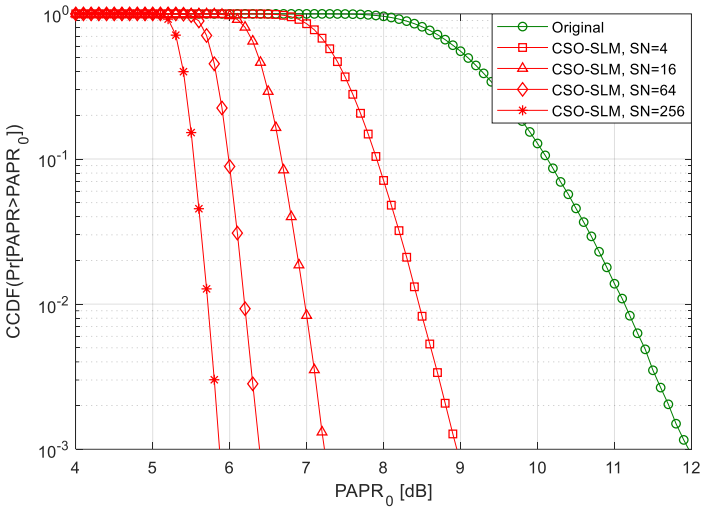

Figure 4. PAPR minimization performance of the CSO-SLM strategy for assorted number of searches.

In Figure 4, with a view to see how the PAPR reduction performance of the CSO-SLM technique is affected by the variation of *SN* value, $PAPR_0$ [dB] – CCDF curve of the relevant scheme was obtained for 4, 16, 64 and 256 search numbers, respectively where $PAPR_0$ signifies the threshold PAPR value and CCDF is the abbreviation of complementary cumulative distribution function expressed by Pr [PAPR > $PAPR_0$]. As can be viewed from the Figure 4, each increment in the value of *SN* brings about a certain enhancement in the PAPR reduction performance of the CSO-SLM technique. Because in each search, the PAPR of transmission signal is tried to be lowered further via a trial of random phase sequence, and the more the number of these trials (the number of searches), the more the PAPR value can be alleviated. For instance, the PAPR improvements obtained in the original signal at CCDF = 10^{-3}

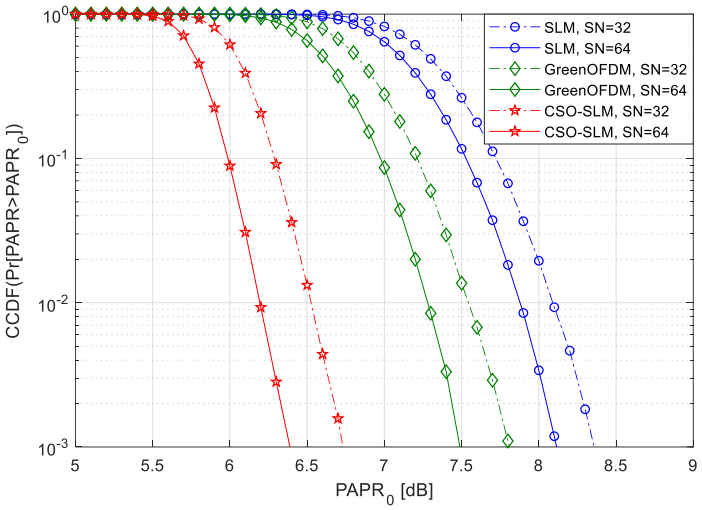

Figure 5. The comparison of PAPR reduction performances shown by the CSO-SLM, GreenOFDM and SLM techniques for varied search numbers.

are equal to 3.01 dB, 4.73 dB, 5.57 dB and 6.09 dB values for *SN* = 4, *SN* = 16, *SN* = 64 and *SN* = 256 search numbers, respectively. As can be figured out from these results, the escalation of search number from 4 to 256 leads to 3.08 dB enhancement in the PAPR improvement achieved in the original signal.

In Figure 5, $PAPR_0$ [dB] – CCDF curves of the CSO-SLM, GreenOFDM and SLM strategies were achieved for 32 and 64 search numbers, respectively and the PAPR reduction performances reached by the relevant techniques in these two different numbers of searches were compared. According to the PAPR curves acquired in Figure 5, it is seen that the CSO-SLM strategy is distinguished, clearly from the other techniques with its predominant PAPR reduction performance. SLM and GreenOFDM methods lagged far behind the CSO-SLM technique in terms of performance for both of the search numbers. For instance, when considering the PAPR curves obtained for *SN* = 32 number of searches, it will be seen that the PAPR values achieved by SLM, GreenOFDM and CSO-SLM techniques at CCDF = 10^{-3} are equal to 8.36 dB, 7.81 dB and 6.73 dB, respectively. According to these results, the CSO-SLM strategy obtains a significantly higher PAPR achievement than the other methods by making a 1.08 dB difference even to its closest competitor, which is the GreenOFDM method.

In Figure 6, in order to observe how much the SLM, GreenOFDM and CSO-SLM techniques can suppress the spectral growths caused by the SSPA, power spectral density curves were obtained for each of the relevant techniques. Alongside the aforementioned PSD curves obtained for 6 dB and 8 dB input back off (IBO) values of the SSPA, the PSD curve that can be achieved in the case that the distortionless amplification is carried out through the linear HPA in the LC-GFDM system was added to the Figure 6 to see the amount of spectral growth caused by the SSPA. In this simulation, the smoothness coefficient of the SSPA and the number of searches for each scheme were determined as *p* = 1 and *SN* = 256, respectively. The PAPR achievement of the CSO-SLM scheme, which is higher than the other methods, reflects also on its power

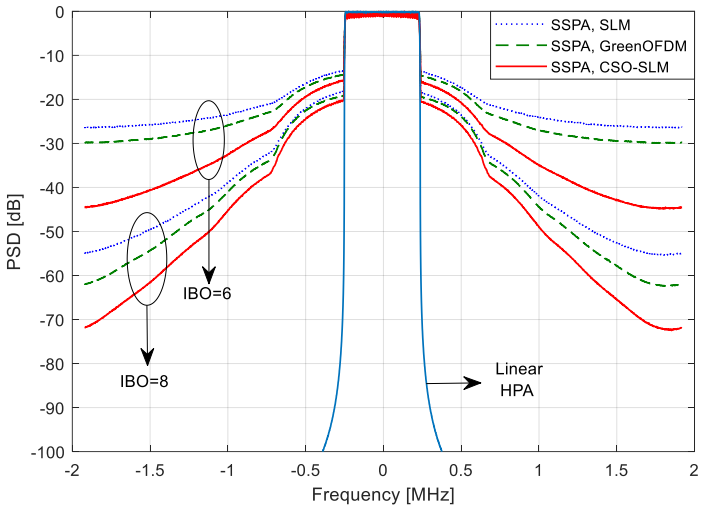

Figure 6. The effects of SLM, GreenOFDM and CSO-SLM techniques on the PSD of LC-GFDM transmission signal.

spectral density performance and makes the related technique to obtain the lowest side lobe level for each IBO value. For instance, for IBO = 6 dB, the CSO-SLM technique reaches −44.51 dB side lobe level, which is the lowest one, by suppressing the SSPA-induced spectral growths 18.18 dB and 14.80 dB more than the SLM and GreenOFDM methods, respectively. Similarly, for IBO = 8 dB, while the lowest PAPR level of −71.77 dB is achieved by the CSO-SLM scheme, it is not possible to get below the −54.81 dB and −61.89 dB levels with the SLM and GreenOFDM methods, respectively.

In Figure 7, CSO-SLM and CSO-PTS techniques are compared with each other in point of PAPR achievements in the LC-GFDM system. To this end, the $PAPR_0$ [dB] – CCDF curves of both techniques were obtained for 4, 16, 64 and 256 search numbers, respectively. As it can be grasped from the explicit differences between the PAPR curves belonging to the relevant techniques, CSO-SLM outperforms the CSO-PTS for each search number. Especially as it is moved from *SN* = 16 towards the higher *SN* values, the performance difference between these two techniques increases even more and reaches its top level at

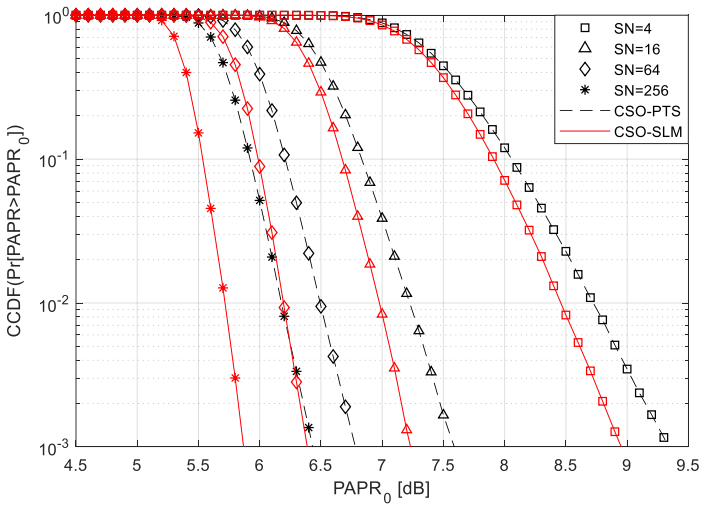

Figure 7. Comparison of PAPR reduction achievements of CSO-SLM and CSO-PTS strategies for varied number of searches.

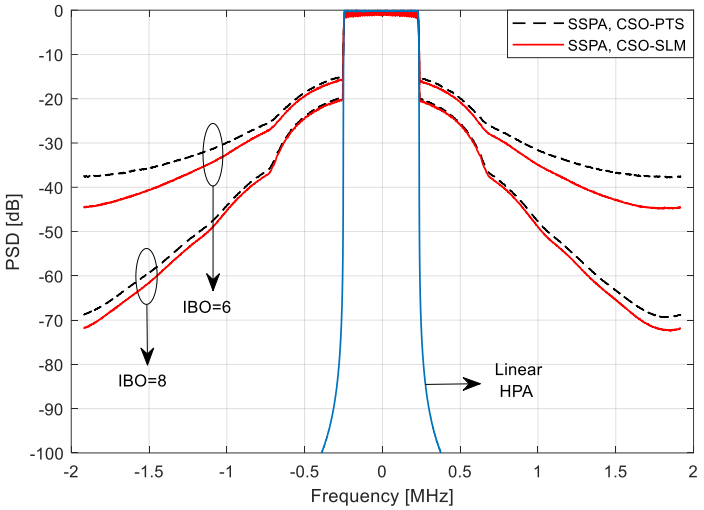

Figure 8. The comparison of PSD performances of CSO-SLM and CSO-PTS strategies for separate IBO values (p = 1, SN = 256).

SN = 256. For example, at CCDF = 10^{-3}, while the PAPR difference between the CSO-PTS and CSO-SLM is 0.36 dB for *SN* = 16, the relating difference reaches 0.55 dB value for *SN* = 256.

In Figure 8, CSO-PTS and CSO-SLM schemes are compared with regard to their effects on the power spectral density of the LC-GFDM transmission signal amplified via SSPA for different IBO values. To that end, the PSD curves of both techniques at 6 dB and 8 dB IBO values were obtained. In addition to the relating PSD curves, power spectral density of the LC-GFDM signal amplified via the linear HPA was added to the Figure 8 as well. As can be figured out from the side lobe levels of the PSD curves acquired for two different IBO values, the spectral growth caused by the SSPA in the high PAPR signals is suppressed further via the CSO-SLM technique. The apparent superiority of the CSO-SLM technique over the CSO-PTS method in terms of PAPR reduction performance engenders significant differences between the side lobe levels of these two techniques. For instance, the side lobe level which can be suppressed down to −37.48 dB via the CSO-PTS is reduced up to the −44.51 dB level with the CSO-SLM technique by fulfilling 7.03 dB more suppression compared to the CSO-PTS method. Even though escalating the IBO value up to the 8 dB brings the side lobe levels of the considered techniques a bit closer together, the CSO-SLM technique reaches the lowest side lobe level with 3.08 dB difference for the relevant IBO value too.

5. Conclusion

In this paper, the conventional SLM scheme, which exhibits an ineffective PAPR reduction performance in the LC-GFDM transmitter due to its vulnerability to the symbol addition process, was upgraded by combining it with the cumulative symbol optimization procedure to develop a new strategy called CSO-SLM that is in no way affected by the addition of GFDM symbols. In order to provide evidence regarding the benefit of the aforementioned modification carried out in the SLM scheme, the proposed CSO-SLM strategy was compared to the classical SLM in point of not only the PAPR achievement, but also the PSD performance. Apart from this, two robust PAPR reduction strategies called GreenOFDM and CSO-PTS were also used as

benchmark techniques in the simulations to be completely sure about the real potential of our proposed method. According to the evident results acquired in the simulation studies, the CSO-SLM strategy unquestionably leaves behind each of the other considered schemes by making quite obvious differences in both PAPR and PSD graphs. As the next step of this study, it is possible to enable the CSO-SLM strategy to reach better PAPR reduction performance with a smaller number of searches by performing phase optimization process via various intelligent optimization algorithms. Apart from this, the CSO procedure, which elevates the PAPR reduction performance of the classical SLM technique in the LC-GFDM waveform, can be integrated to different classical methods to develop new PAPR reduction strategies for the related waveform.

Acknowledgement

This study was supported by the Scientific Research Projects Coordination Unit of Erciyes University [Grant No: FDK-2018-8463].

References

Barba-Maza, L. M., & Dolecek, G. J. (2020, August 9-12). *PAPR reduction of GFDM system using Xia pulse and OPTS scheme* [Conference presentation]. IEEE 63rd International Midwest Symposium on Circuits and Systems (MWSCAS), Springfield, MA, USA.

Bauml, R. W., Fischer, R. F. H., & Huber, J. B. (1996). Reducing the peak-to-average power ratio of multicarrier modulation by selected mapping. *Electronics Letters*, 32(22), 2056-2057.

Chen, J. C., & Wen, C. K. (2010). PAPR reduction of OFDM signals using cross-entropy-based tone injection schemes. *IEEE Signal Processing Letters*, 17(8), 727-730.

Cimini, L. J., (1985). Analysis and simulation of a digital mobile channel using orthogonal frequency division multiplexing. *IEEE Transactions on Communications*, 33(7), 665-675.

Cimini, L. J., & Sollenberger, N. R. (2000). Peak-to-average power ratio reduction of an OFDM signal using partial transmit sequences. *IEEE Communications Letters*, 4(3), 86-88.

Fettweis, G., Krondorf, M., & Bittner, S. (2009, April 26-29). *GFDM - generalized frequency division multiplexing* [Conference presentation]. VTC Spring 2009 - IEEE 69th Vehicular Technology Conference, Barcelona, Spain.

Güner, A. (2022). Evre uyumlu optik OFDM sistemler için karmaşık aşırı öğrenme makinası tabanlı doğrusal olmayan denkleştirici. *European Journal of Science and Technology*, (33), 26-31.

Jayalath, A. D. S., & Tellambura, C. (2000). Reducing the peak-to-average power ratio of orthogonal frequency division multiplexing signal through bit or symbol interleaving. *Electronics Letters*, 36(13), 1161-1163.

Jayati, A. E., Wirawan, W., Suryani, T., & Endroyono, E. (2019). Partial transmit sequence and selected mapping schemes for PAPR reduction in GFDM systems. *International Journal of Intelligent Engineering and Systems*, 12(6), 114-122.

Jones, A. E., Wilkinson, T. A., & Barton, S. K. (1994). Block coding scheme for reduction of peak to mean envelope power ratio of multicarrier transmission schemes. *Electronics Letters*, 30(25), 2098-2099.

Krongold, B. S., & Jones, D. L. (2003). PAR reduction in OFDM via active constellation extension. *IEEE Transactions on Broadcasting*, 43(3), 258-268.

Krongold, B. S., & Jones, D. L. (2004). An active-set approach for OFDM PAR reduction via tone reservation. *IEEE Transactions on Signal Processing*, 52(2), 495-509.

Li, X., & Cimini, L. J. (1998). Effect of clipping and filtering on the performance of OFDM. *IEEE Communications Letters*, 2(5), 131-133.

Matthé, M., Mendes, L., Gaspar, I., Michailow, N., Zhang, D., & Fettweis, G. (2016). Precoded GFDM transceiver with low complexity time domain processing. *EURASIP Journal on Wireless Communications and Networking*, 2016(1), 1-9.

Mestdagh, D. J. G., GulfoMonsalve, J. L., & Brossier, J. M. (2018). GreenOFDM: a new selected mapping method for OFDM PAPR reduction. *Electronics Letters*, 54(7), 449-450.

Michailow, N., Datta, R., Krone, S., Lentmaier, M., & Fettweis, G. (2012). *Generalized frequency division multiplexing: a flexible multi-carrier modulation scheme for 5th generation cellular networks* [Conference presentation]. German Microwave Conference (GeMiC), Ilmenau, Germany.

Michailow, N., Krone, S., Lentmaier, M., & Fettweis, G. (2012, September 3-6). *Bit error rate performance of generalized frequency division multiplexing* [Conference presentation]. IEEE Vehicular Technology Conference (VTC Fall), Quebec City, Canada.

Michailow, N., Matthé, M., Gaspar, I. S., Caldevilla, A. N., Mendes, L. L., Festag, A., & Fettweis, G. (2014). Generalized frequency division multiplexing for 5th generation cellular networks. *IEEE Transactions on Communications*, 62(9), 3045-3061.

Paredes, M. C. P., Grijalva, F., Rodrigez, J. C., & Sarzosa, F. (2017, October 16-20). *Performance analysis of the effects caused by HPA models on an OFDM signal with high PAPR* [Conference presentation]. IEEE Second Ecuador Technical Chapters Meeting (ETCM), Salinas, Ecuador.

Ryu, H. G., Park, J. S., & Park, J. S. (2004). Threshold IBO of HPA in the predistorted OFDM communication system. *IEEE Transactions on Broadcasting*, 50(4), 425-428.

Sim, Z. A., Reine, R., Zang, Z., Juwono, F. H., & Gopal, L. (2019, April 28-May 1). *Reducing the PAPR of GFDM systems with quadratic programming filter design* [Conference presentation]. IEEE 89th Vehicular Technology Conference (VTC2019-Spring), Kuala Lumpur, Malaysia.

Şimşir, Ş., & Taşpınar, N. (2020). Cumulative symbol optimization-based partial transmit sequence technique for PAPR reduction in low complexity GFDM system. *Transactions on Emerging Telecommunications Technologies*, 31(6), 1-19.

Taşpınar, N., & Şimşir, Ş. (2020). Bio-inspired pilot design approach based on genetic algorithm for OFDM-IDMA scheme. *European Journal of Science and Technology*, (19), 466-474.

Tiwari, S. O., & Paulus, R. (2020). Non-linear companding scheme for peak-to-average power ratio (PAPR) reduction in generalized frequency division multiplexing. *Journal of Optical Communications*, DOI: https://doi.org/10.1515/joc-2020-0174.